ELSEVIER

Nuclear Instruments and Methods in Physics Research A 439 (2000) 497–506

NUCLEAR INSTRUMENTS & METHODS IN PHYSICS RESEARCH Section A

www.elsevier.nl/locate/nima

Silicon drift detectors for the STAR/SVT experiment at RHIC

STAR-SVT Collaboration

J. Takahashi[a,*], R. Bellwied[b], R. Beuttenmuller[c], H. Caines[d], W. Chen[c], D. DiMassimo[c], H. Dyke[d], D. Elliot[c], M. Grau[c], G.W. Hoffmann[e], T. Humanic[d], P. Jensen[e], I.V. Kotov[d], H.W. Kraner[c], P. Kuczewski[c], W. Leonhardt[c], Z. Li[c], C. Liaw[c], G. LoCurto[d], D. Lynn[c], N. Mazeh[b], P. Middelkamp[c], R. Minor[f], S. Nehmeh[b], G. Ott[c], S.U. Pandey[b], D. Pinelli[c], C. Pruneau[b], V.L. Rykov[b], J. Schambach[c], J. Sedlmeir[c], J. Sheen[b], R. Soja[c], D. Stefani[c], E. Sugarbaker[d], W.K. Wilson[b]

[a]*Universidade de São Paulo, São Paulo, Brazil*
[b]*Wayne State University, Detroit, MI 48201, USA*
[c]*Brookhaven National Laboratory, Upton, NY 11973, USA*
[d]*Ohio State University, Columbus, OH 43210, USA*
[e]*University of Texas, Austin, TX 78712, USA*
[f]*Lawrence Berkeley Laboratory, Berkeley, CA 94720, USA*

Abstract

Large-area linear Silicon Drift Detectors (SDD) were developed to be used in the Silicon Vertex Tracker (SVT) of the STAR experiment at the BNL Relativistic Heavy Ion Collider (RHIC). The design of the SDD has been finalized and submitted for large-scale production. Test results show that the detector exhibits excellent position resolution and low noise. A special characterization procedure was developed to test detector wafers in order to select good detectors for the SVT. Recently, 15 STAR/SVT SDDs were assembled as a tracking device in a BNL-AGS heavy-ion experiment (E896). This was the first tracking application of these detectors and their corresponding front-end electronics in an experimental environment. Preliminary results indicating good detector performance are shown and discussed in this paper.

1. Introduction

Silicon Drift Detectors (SDD) [1,2] provide unambiguous two-dimensional position information for charged particle detection in a single detector layer. The operating principle of the SDD is based upon creating a drift channel inside the depleted silicon wafer. This combines the advantages of a semiconductor detector (e.g. high ionization efficiency) with some of the best features of gas drift chambers (e.g. low number of readout channels). By measuring the drift time together with the distribution of signals along the readout anodes, position

* Correspondence address: Brookhaven National Laboratory, Instrumentation Division, Bldg. 535B, P.O. Box 500, Upton, NY 11973-5000, USA.

E-mail address: jtakahas@physics.wayne.edu (J. Takahashi)

0168-9002/00/$ - see front matter
PII: S0168-9002(99)00918-3

information can be obtained in both dimensions. The high spatial resolution, at a cost effective granularity, make these devices ideal tracking detectors.

A large-area linear SDD was developed to be used in the Silicon Vertex Tracker (SVT), the inner tracking detector for the Solenoidal Tracker at RHIC (STAR) experiment [3]. The SVT consists of 216 silicon drift detectors, each with an area of 6.3 $\times$ 6.3 cm^2, mounted on three concentric barrels. Wafers are mounted onto beryllium ladder structures holding either 4, 6 or 7 detectors depending on the barrel number. The ladders are arranged in polygon-shaped barrels with 8, 12 and 16 ladders each to surround the colliding beams and their point of interaction at radii of 6.6, 10.6 and 14.5 cm, respectively.

The final detector design minimized the inactive area and improved the position resolution in order to maximize the tracking efficiency. In addition, optimization of the implanted structures improved the robustness of the processing and thus increased the production yield as well as the detector performance during actual experimental running conditions. In this paper, we first describe detector layout characteristics and document the motivation for SDD selection criteria. Finally, we show the latest performance results based on two important system tests.

2. STAR silicon drift detector final design

The STAR-SVT SDD's are produced using a 4 in diameter, 280 μm thick, neutron transmutation doped (NTD) silicon wafer with an approximate resistivity of 3 kΩ cm. The detector part of the wafer has dimensions of 6.3×6.3 cm^2 and is divided into two symmetrical drift directions. In each drift direction, 220 p^+ cathode strips are implanted on both surfaces with a spatial pitch of 135 μm. A section of the detector design is detailed in Fig. 1.The cathode strips are connected in series through implanted resistors to gradually reduce the negative potential from the center of the detector towards the edge, where the charge collection anodes are placed. An aluminum overlay, wider than the p^+ implant strips, covers each cathode to reduce the electric

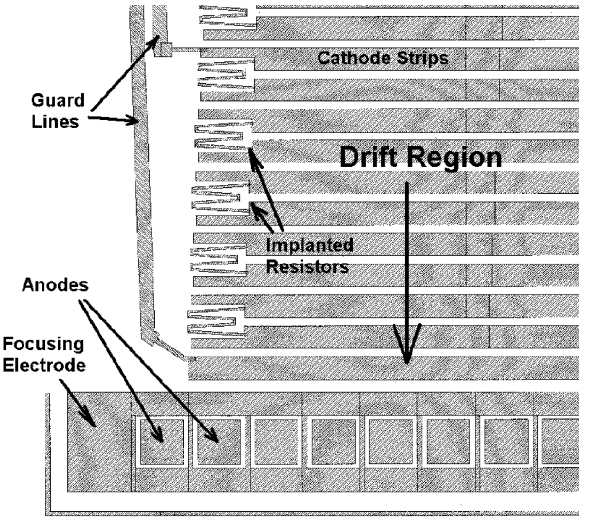

Fig. 1. Schematic view of a section of the detector, near the charge collection region.

fields at the junction between the implanted region and the oxide.

On the lateral sides of the detector, guard lines connected to every 10th cathode reduce the potential at the edge of the detector. The design of the guard area was optimized to reduce leakage currents and avoid voltage breakdowns, thus maintaining the voltage linearity of the cathodes. The area occupied by the guard lines was kept to a minimum to optimize tracking efficiency. The active area corresponds to 94.5% of the total detector.

In the charge collection region, 240 n^+ implanted anodes, 250 μm apart, are surrounded by focusing cathodes. Electrons drifting in the active detector area are forced towards the anodes on the surface by the field generated by the focusing electrodes. Detectors from earlier prototypes have shown to be very sensitive to voltage variations of these focusing electrodes. So in the final design, modifications of the focusing region design improved the charge collection uniformity [9]. For example, the "gaps" between electrodes were minimized to reduce potential wells near the detector surface that could trap the incoming electrons before they reach the anodes.

For drift velocity calibration, eight MOS-type charge injection lines (four on each drift direction)

Table 1
Summary of STAR/SVT-SDD prototypes production

Detector design	Year	Produced by	Quantity produced	Yield (%)
STAR-1.0	1992	BNL	10	40
STAR-2.0	1993	BNL	12	30
STAR-2.5	1994	BNL	08	50
STAR-2.7	1995–1996	BNL + SINTEF[a]	56	60
STAR-2.8	1996–1997	BNL	08	40
STAR-2.9	1997	BNL + SINTEF	50	75
STAR-2.9	1998	BNL + SINTEF	250	70
STAR-2.9	1999	BNL + SINTEF	350 (expected)	70

[a]SINTEF is a commercial wafer producing facility.

were implemented between adjacent cathode strips at drift distances of 0.2, 1.0, 2.0 cm and at the maximum drift distance of 3.0 cm [5–7]. Further details of the detector design and fabrication can be found in Refs. [8,9].

In the development of the final detector design, the aim was not only to optimize the detector performance, but also to make the detector design sufficiently robust to increase the production yield. Delicate and thin structures that are sensitive to the etching step of the detector processing were avoided in the design development. In addition, small oxide gaps, such as the barrier between the anodes and the focusing electrode (approximately 10 μm) were increased to reduce the risk of possible voltage breakdowns. Table 1 summarizes the quantities and yields of the previous STAR/SDD production, as well as projections for future production. Note the generally increasing production yield with subsequent design iterations. Approximately 250 wafers are required to complete the STAR/SVT detector. The final version of the silicon drift detector described here is now in production.

3. Production mode selection criteria

In large detector systems, such as the SVT, which are composed of several single detectors, it is important to verify that every detector meets specifications. Inactive or noisy wafers considerably reduce the tracking efficiency and replacement of single wafers once the SVT is assembled is difficult. Thus a non-destructive, low-cost testing procedure was developed to evaluate the quality of each wafer before selection for the SVT assembly. Wafers are tested on probe stations, where microscopic probes make electrical contact to both surfaces of the detector, allowing one to bias the detector without wire bonding. With this method it is possible to test large quantities of wafers in a limited amount of time.

The complete testing procedure can be separated into three main steps: visual inspection, test structure measurements, and active region measurements. Visual inspection is performed during and after the processing of the detectors. During the fabrication, wafers are inspected between each major processing step. Standard defects such as ohmic bridges between electrodes or mask alignment errors are searched for and in many cases it is possible to redo certain processing steps. Once the detector is fabricated, a final visual inspection is performed. Due to the previous inspections, the rejection rate at this point is very low (below 5% for the wafers that have passed all previous visual inspections).

The next step of the selection procedure consists of measurements performed on the test structures. Small structures such as implanted resistor chains, p–n diode junctions and MOS capacitors were implemented on the outer edges of the wafer, surrounding the detector. I–V and C–V measurements from these test structures provide information of the oxide charge density, the implanted resistors values and p–n junction reverse leakage

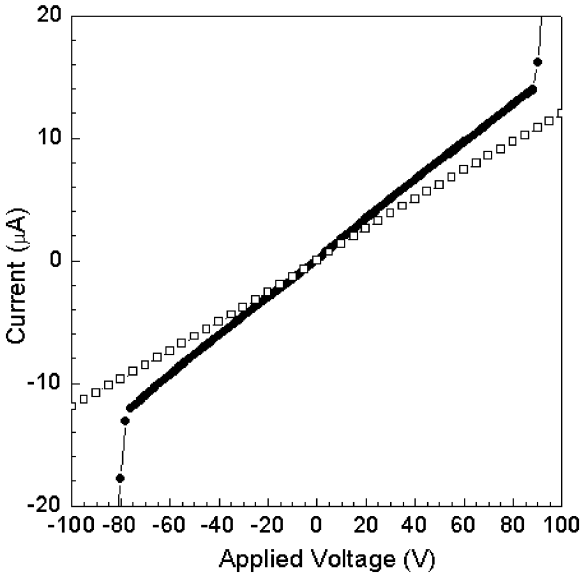

Fig. 2. Typical I–V curve from resistor series test structures. Currents are measured from -100 to $+100$ V for a series made of 10 implanted resistors.

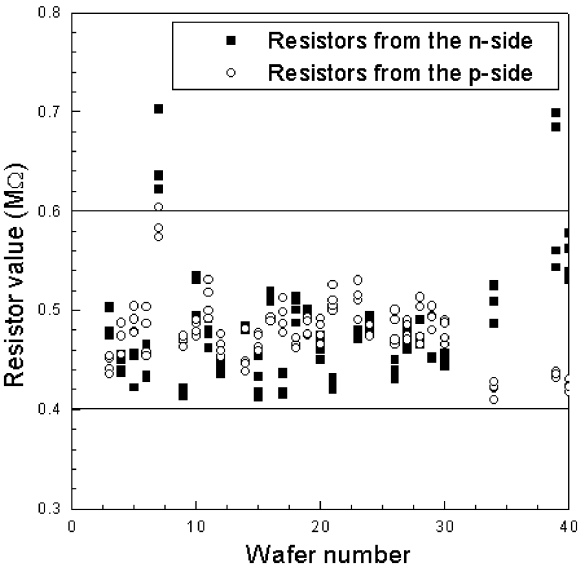

Fig. 3. Summary of resistor test structure values measured from 27 detectors produced in the same batch. Horizontal lines indicate the criterion limits of 500 $\pm$ 100 kΩ.

current. These parameters are used to evaluate the detector processing quality. Fig. 2 shows I–V curves from resistor chain test structure measurements. The curve with the open squares shows the expected behavior, the other curve (with solid circles) shows a voltage breakdown for bias values above ± 80 V. These voltage breakdowns may occur due to surface currents, which are correlated to the density of charges accumulated at the Si/SiO_2 interface. For the SVT, the maximum bias on the detector is equivalent to a voltage difference of 7 V per resistor that corresponds to ± 70 V on the scale of Fig. 2. To provide a safety margin, the resistor chain is required to sustain voltages up to ± 100 V.

If a resistor value is too high the voltage distribution becomes too susceptible to leakage currents. On the other hand, if the resistor value is too low, heat dissipation affects the drift uniformity. For the chosen value of 500 kΩ, simulations show a maximum temperature gradient of 0.3 K. Fig. 3 shows a summary of the test structure resistance measurements for a batch of 27 STAR detectors. The straight horizontal lines represent the limits of the selection criteria. The limits were defined considering processing capabilities, production yields and detector performance.

Fig. 4 shows a typical I–V curve measured on a reverse biased diode test structure. The diode leakage current provides information on the expected leakage current and it is also correlated to the carrier lifetime. The selection criterion requires a leakage current of less than 250 pA/mm^2 at a reverse bias of 100 V. This current value corresponds to a carrier lifetime for electrons of approximately 11 ms in 3 kΩ cm silicon at room temperature. The total leakage current from a cathode strip, considering a diode leakage current of 250 pA/mm^2, is approximately 2 nA. This would correspond to a voltage non-linearity of less than 0.2 %. Diode leakage current results from 27 detectors are shown in Fig. 4. Diode C–V measurements and MOS capacitor Flat Band voltage shift measurements are also performed on the test structures, but not shown here. Based on present detectors statistics, about 80% of all wafers that passed the visual inspection also pass the test structure measurements (Fig. 5).

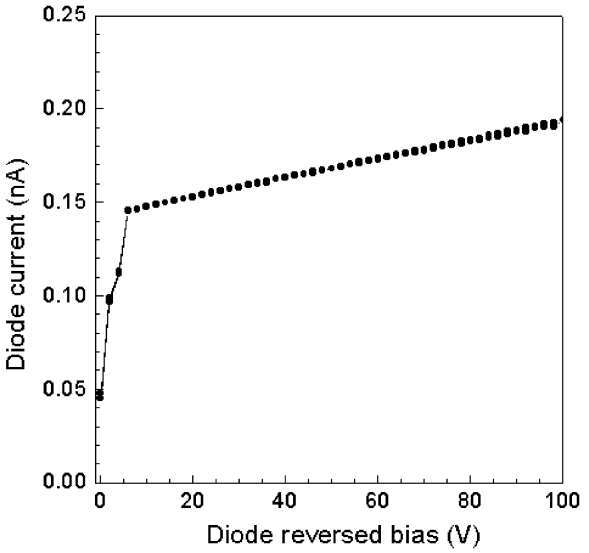

Fig. 4. Typical I–V measurement from a p–n diode junction test structure. Maximum leakage current is required to be below 250 pA/mm^2, at a reverse bias of 100 V. Diode area is 4 mm^2.

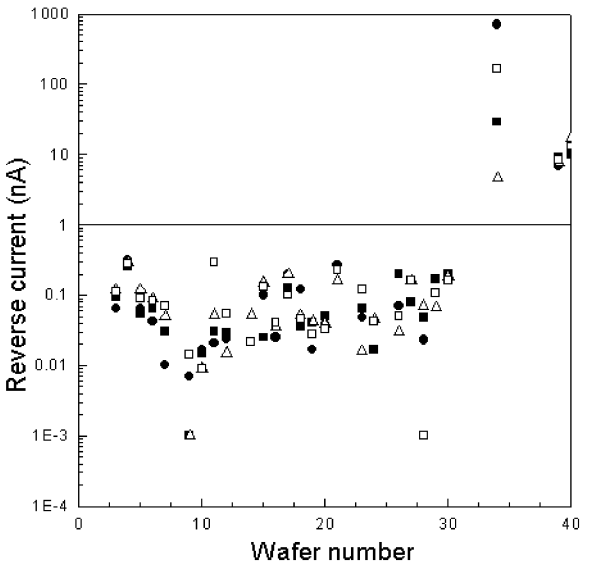

Fig. 5. Summary of diode test structure current measurements at a reverse bias of 100 V. The horizontal line indicates the maximum current limit of 1 nA.

The final selection procedure is based on tests performed on the active part of the wafer, i.e. the detector itself. Electrical measurements are performed using a special probe station. In order to

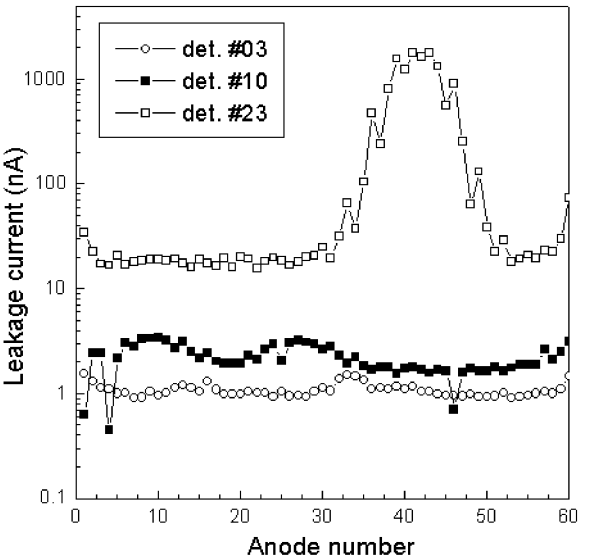

Fig. 6. Typical results from DC current measurement for 60 anodes from three different detectors measured on the probe station.

bias cathodes of both sides of the detector, the uncut wafer is kept in a vertical position, and on each side a 6 cm long probe card, with 25 probes make electrical contact with the surface of the detector, biasing the cathodes up to 1000 V. Voltage linearity and guard anode currents are measured as a function of detector bias. Anode leakage current is measured using a 120-probe test card. Fig. 6 shows typical results. In this example, two wafers have anode leakage currents below the maximum acceptable value of 150 nA, and one detector (# 23) shows a region with high leakage current. The limit of 150 nA is stipulated by the readout electronics noise specifications. Fig. 7 shows a summary of the average anode leakage currents from a batch of 27 detectors.

In summary, after performing all three test series (visual, test structure and active area measurements), from 27 detectors, 7 detectors failed to meet the selection criteria, resulting in a production yield of approximately 75%.

4. Performance of the final SVT detector design

During commercial production, a few detectors per batch are selected to be mounted on special

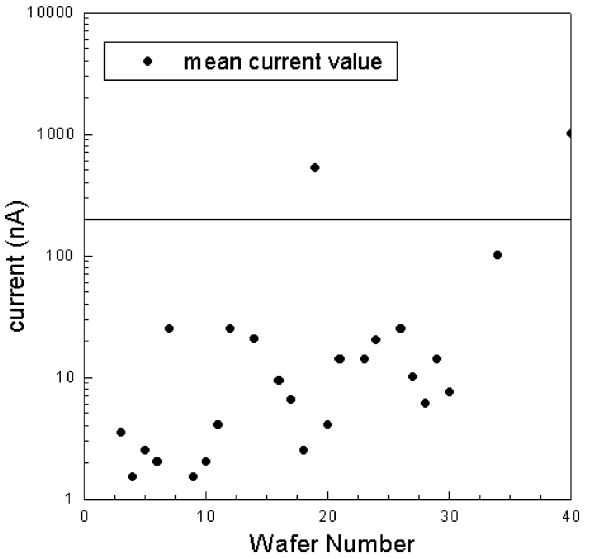

Fig. 7. Summary of the average anode leakage current measured on the probe station with detectors biased at 1000 V.

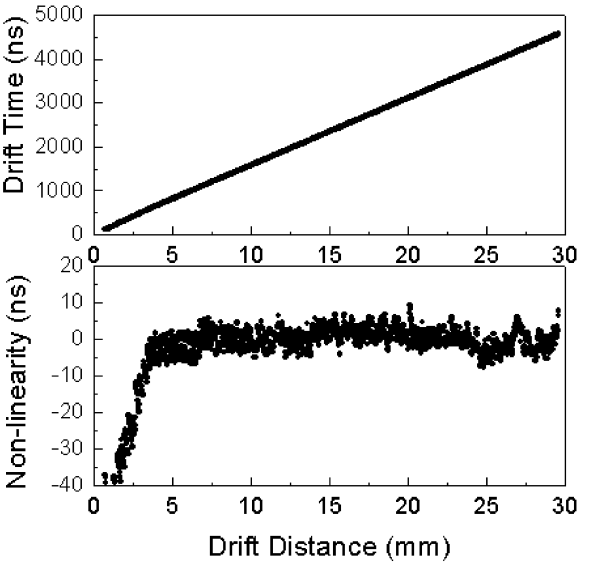

Fig. 8. Drift time as a function of drift distance, measured on the laser test station.

testing PC boards for more detailed measurements. Laser injection through a microscope is used to ionize charges in a small spot (RMS width of 20 μm) on the detector, simulating a charged particle passing through the detector. Drift linearity curves are measured using an automated $X-Y$ stage that moves the laser spot on the detector.

Fig. 8 shows a typical result for a drift time and drift non-linearity measurement. Below a drift distance of approximately 3.0 mm, there is a change in the drift velocity that is caused by the intentional voltage difference between the n-side and the p-side of the focusing region of the detector (between cathode 20 and the anodes). Fig. 9 shows a histogram of the drift non-linearity calculated with respect to a linear fit to the data above a drift distance of 3.0 mm. In this example the non-linearity has a standard deviation of approximately 2.9 ns, corresponding to a position non-linearity of approximately 20 μm, which is typical for most SVT detectors. Based on a large sample of non-linearity measurements performed on various detectors, it was determined that the drift non-linearities are uniform across the anodes, therefore a non-uniformity measurement of a few anodes is sufficient to "map" the effect.

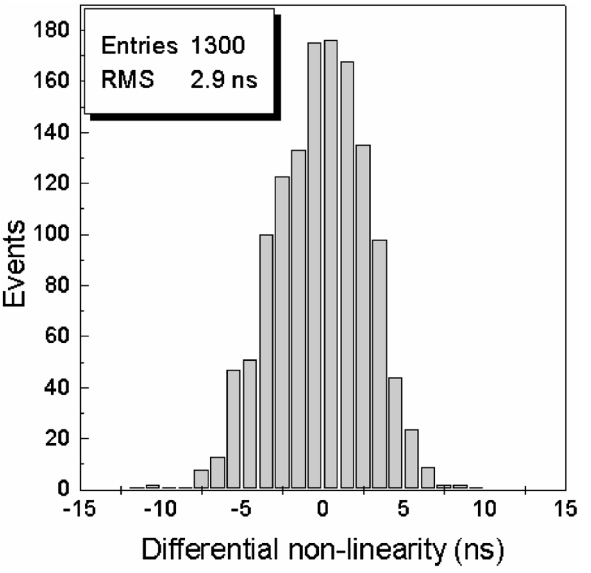

Fig. 9. Distribution of the drift non-linearities calculated from the deviation from a linear fit for drift distances above 3.0 mm.

Position accuracy in the drift direction is determined by taking a series of drift time measurements with the laser at fixed positions. The position of the laser on the detector was measured 100 times and

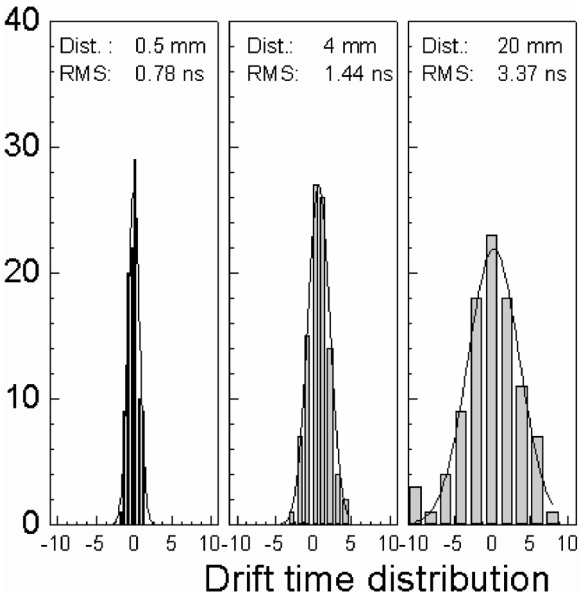

Fig. 10. Scatter in the drift time measurement for three different drift distance. For each position, the measurement was sampled 100 times.

histogramed. Fig. 10 shows the distribution of the position measurements for three different drift distances. The change in the accuracy with drift distance indicates that there are systematic effects that degrade the position accuracy, such as drift non-linearities and the decrease of the signal-to-noise ratio for longer drift distances. The measured accuracy at the shortest drift distance corresponds to the best position accuracy achievable with this detector design. The drift time RMS of 0.78 ns at a drift velocity of 6.2 μm/ns (500 V/cm) translates to a position accuracy of approximately 5 μm. The 3.37 ns width for long drift distances corresponds to an accuracy of about 21 μm. On average the position resolution in the drift direction is below 20 μm.

In addition to the measurements taken under controlled laboratory conditions, SVT detectors were also used in a heavy-ion experiment at the AGS accelerator at Brookhaven National Laboratory. E896 is a heavy-ion fixed target experiment measuring ^{197}Au + ^{197}Au collisions at energy of 11.6 GeV/c per nucleon [11,12]. The main physics motivation for this experiment is the search for the H_0 dibaryon, a 6-quark state which is postulated to

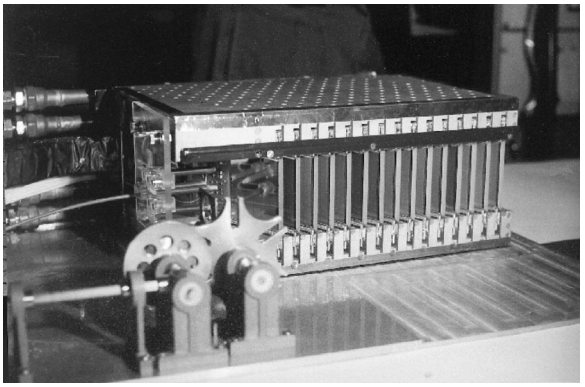

Fig. 11. Picture of the Silicon Drift Detector Array used in the April 1998 beam run of AGS-BNL experiment 896.

exist [13]. The experiment also has high sensitivity for short-lived particles with strange quark content such as Λ, $\bar{\Lambda}$, and Ξ. This sensitivity is achieved by using an array of STAR-SVT SDD for charged particle tracking and vertexing. The actual wafers were chosen using the selection criteria described in this paper. The array was positioned near the interaction target, inside a superconducting magnet that generated a 6.2 T field. Detectors and their corresponding front-end electronics [4] were mounted on custom printed circuit boards. Detectors were biased through an external voltage divider mounted on the PC-boards and connected via wire bonds to every 10th cathode of both surfaces. Front-end electronics assembled on a hybrid carrier were placed on both sides of the detector, aligned with the anodes and fixed using heat conductive epoxy. Each anode on the detector was connected to an input channel of the pre-amplifier/shaper (PASA) through wire bonds. The 15 PC-boards with detectors and front-end hybrids were positioned inside the magnet by a water-cooled aluminum support structure. Fig. 11 shows a picture of the setup. Data were acquired using the same readout electronics and data-acquisition system to be used in the SVT. Approximately one million events were recorded over 25 d of data taking. During this period, on-line monitoring software was used to view raw events, display hits on the detectors and calculate detector pedestals, noise levels and fluctuations. In addition, a slow control

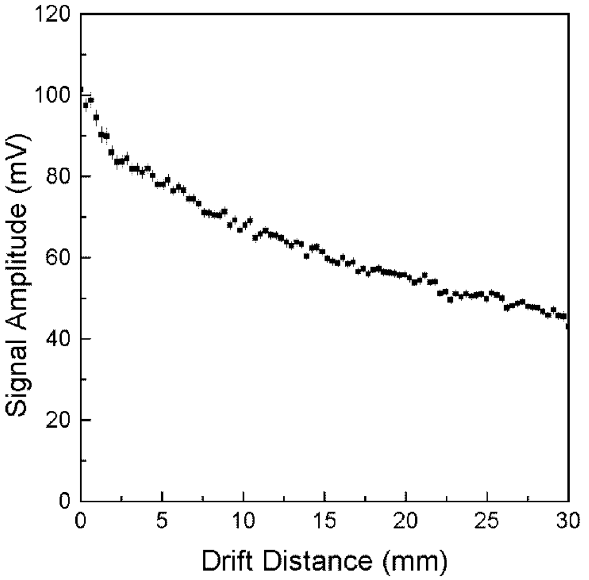

Fig. 12. Measured cluster amplitude (highest pixel) as a function of drift distance.

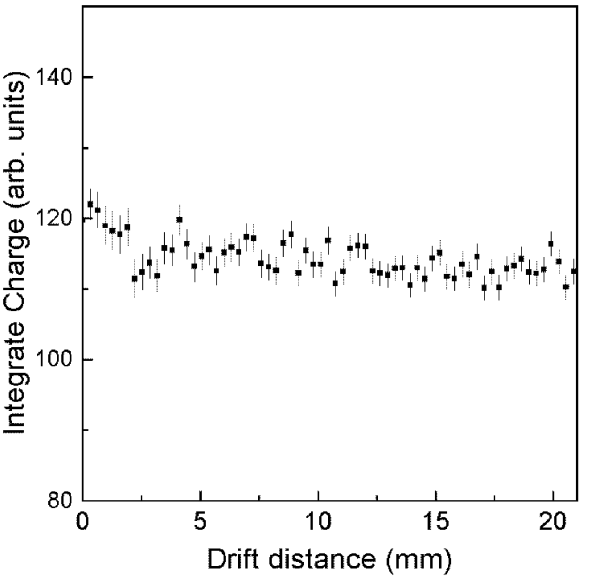

Fig. 13. Most probable value of the summed ADC (total charge) in arbitrary units as a function of drift distance.

system monitored detector parameters such as guard anode current and temperature.

For reconstructed hits, the measured hit amplitude as a function of drift distance for 100 events is shown in Fig. 12. Each point of the scatter plot corresponds to a hit cluster amplitude. As expected, the signal amplitude decreases with drift distance due to the diffusion of the electron cloud. Fig. 13 shows the integrated charge of the measured cluster as a function of the drift distance. This result indicates that the collected charge is independent of the drift distance.

The hit occupancy per event as a function of the detector coordinate in the transverse (anode) direction and in the longitudinal (drift) direction are shown in Figs. 14 and 15, respectively. The solid circles represent the expected occupancy based on simulations. The good agreement between the experimental data and the simulation indicates good hit detection efficiency.

Fig. 16 shows the number of hits measured in a single plane of the SDDA as a function of the event centrality (multiplicity) that was determined by a scintillation detector used in the experiment. The linear behavior of this dependence indicates

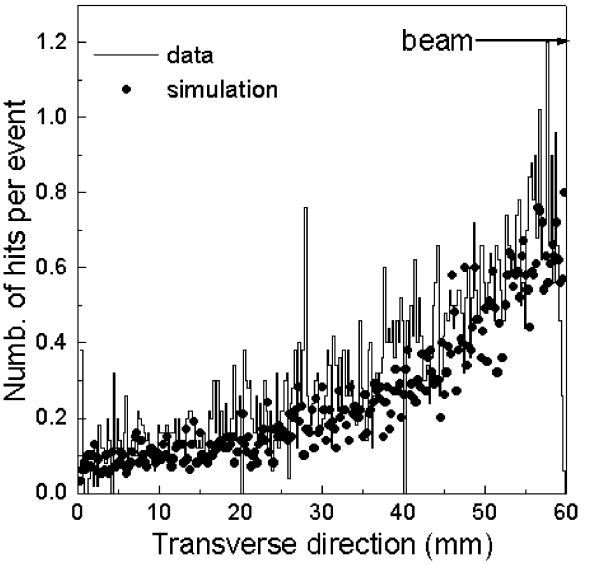

Fig. 14. Detector hit occupancy in the transverse direction (histogram), compared to the expected occupancy from the simulation (solid circles).

that the number of hits increase proportionally with the centrality of reaction, with no evidence of any saturation for large detector occupancies. For

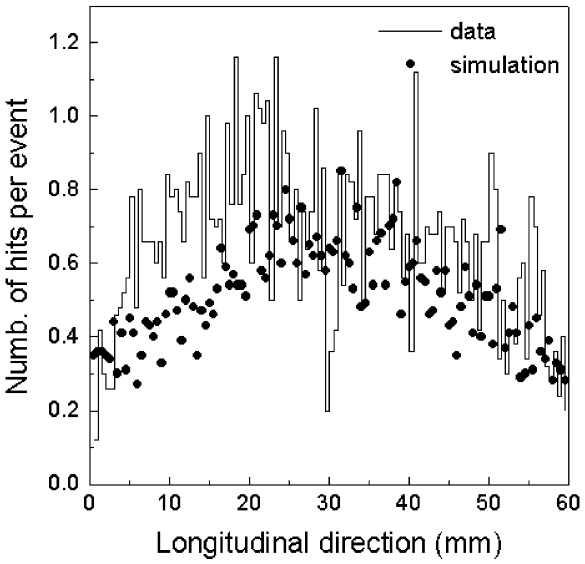

Fig. 15. Detector hit occupancy in the longitudinal direction (histogram), compared to the expected occupancy from the simulation (solid circles).

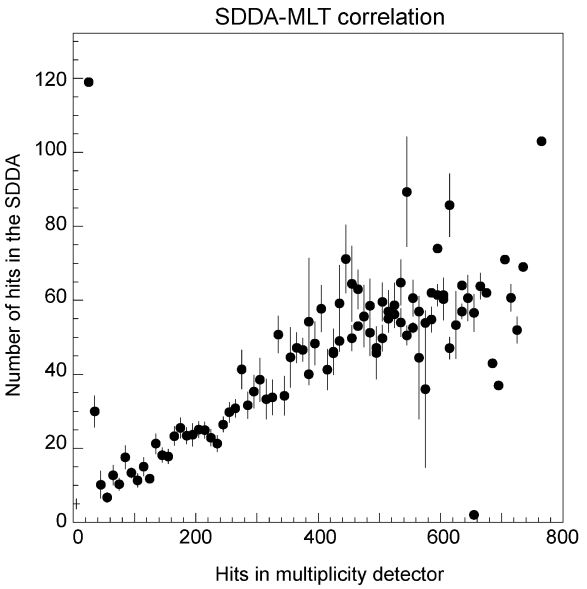

Fig. 16. Relation between the number of hits measured in one Silicon Drift Detector used in the AGS-E896 experiment and the reaction centrality, measured by a scintilator detector.

central collisions an average of 60 hits per event is measured on each detector.

Finally, E896 provided a realistic environment to study the effects of temperature and magnetic field on the drift detector performance. The extremely high and relatively homogeneous magnetic field achievable with the super-conducting magnet in E896 provided a unique opportunity to study effects of the magnetic field on the electron drift. Besides Hall effects, due to changes in the silicon lattice characteristics in a magnetic field, a magneto-resistance effect is also expected [10]. A related data analysis will be presented in a future paper. The ambient temperature was measured during the data acquisition with a thermistor mounted near each detector. The measured correlation between drift velocity and the temperature is in accordance with earlier results presented in Ref. [8].

5. Conclusions

Recently, the detector design for the STAR-SVT SDD was finalized and submitted for commercial production. Tests in the laboratory, such as laser drift measurements and anode leakage current measurements show that the detectors exhibit excellent position resolution and low noise levels. The charge collection efficiency is also high.

Large-scale production of these detectors has started aiming at producing the total of 250 wafers required for the SVT. Due to the large quantity of wafers to be tested, and the high quality requirements of the SVT, a non-destructive testing procedure was developed to characterize and select the wafers. Testing stations in two different institutions are capable of testing up to three detector wafers per day. Selection criteria have been established on the basis of detector performance requirements.

In a recent heavy-ion experiment (AGS-E896) 15 SDDs were assembled and used as a tracking device in a high magnetic field environment. Preliminary results indicate low noise levels and no evidence of charge recombination or hit loss. The total number of dead channels was around 1%, which is well below the SVT requirement of 2%.

Acknowledgements

This work is supported in part by the US Department of Energy (under contract No. DE-AC02-98CH10886 and DE-FQ02-92ER40713), the National Science Foundation (under grant PHY-9511850), and the Robert A. Welch Foundation.

References

[1] E. Gatti, P. Rehak, Nucl. Instr. and Meth. 225 (1984) 608.
[2] P. Rehak et al., Nucl. Instr. and Meth. A 235 (1985) 224.
[3] J.W. Harris, the STAR Collaboration, Nucl. Phys. A 566 (1994) 277c.
[4] D. Lynn et al., Nucl. Instr. and Meth. A 439 (2000) 418.
[5] R. Bellwied et al., Nucl. Instr. and Meth. A 426 (1999) 70.
[6] P. Rehak et al., Electron injection in semiconductor drift chambers, Conference Record IEEE NSS, Vol. 1, Arlington, VA, October 22–27, 1990, pp. 41–45.
[7] E. Gatti et al., Nucl. Instr. and Meth. A 295 (1990) 489.
[8] R. Bellwied et al., STAR/SVT Collaboration, Nucl. Instr. and Meth. A 377 (1996) 387.
[9] R. Bellwied et al., Nucl. Instr. and Meth. A 400 (1997) 279.
[10] S. Pandey et al., STAR/SVT Collaboration, Nucl. Instr. and Meth. A 283 (1996) 537.
[11] H. Crawford, T.J. Hallman et al., Proposal 896 for BNL-AGS, Search for short-lived H dibarion, short-lived strange matter, and to investigate hyperon production in 11.6 GeV/c/N Au + Au collisions.
[12] W.J. Lope et al., The BNL-AGS Experiment 896, Proceedings of the 12th Winter Workshop on Nuclear Dynamics, Snowbird, Utah, Plenum Press, New York, 1996.
[13] R.L. Jaffe, Phys. Rev. Lett. 38 (1977) 195.